Signal Processing 90 (2010) 848–859

Contents lists available at ScienceDirect

Signal Processing

journal homepage: www.elsevier.com/locate/sigpro

A super-resolution reconstruction algorithm for surveillance images

Liangpei Zhang [a,*], Hongyan Zhang [a], Huanfeng Shen [b], Pingxiang Li [a]

[a] The State Key Laboratory of Information Engineering in Surveying, Mapping and Remote Sensing, Wuhan University, Wuhan, Hubei, China
[b] School of Resource and Environmental Science, Wuhan University, Wuhan, Hubei, China

ARTICLE INFO

Article history:
Received 18 November 2008
Received in revised form
28 August 2009
Accepted 3 September 2009
Available online 23 September 2009

Keywords:
Super-resolution
Surveillance images
MAP
CG

ABSTRACT

In many surveillance video applications, it is of interest to recognize a region of interest (ROI), which often occupies a small portion of a low-resolution, noisy video. This paper proposes an edge-preserving maximum *a posteriori* (MAP) estimation based super-resolution algorithm using a weighted directional Markov image prior model for a ROI from more than one low-resolution surveillance image. Conjugate gradient (CG) optimization based on standard operations on images is then developed to improve the computational efficiency of the algorithm. The proposed algorithm is tested on different series of surveillance images. The experimental results indicate that the proposed algorithm has considerable effectiveness in terms of both objective measurements and visual evaluation.

1. Introduction

High-resolution (HR) images are useful in many applications such as surveillance, video frame freezing, medical diagnostics, and military information gathering, etc. However, because of the high cost and physical limitations of the high precision optics and image sensors, it is not easy to obtain the desired HR images in many cases. Therefore, super-resolution (SR) image reconstruction techniques, which can reconstruct one or a set of HR images from a sequence of low-resolution (LR) images of the same scene, have been widely researched in the last two decades.

Super-resolution image reconstruction refers to a process that produces a HR image from a sequence of LR images. It overcomes the inherent resolution limitation by bringing together the additional information from each image. Generally, SR techniques can be divided into frequency domain algorithms and spatial domain algorithms. Much of the earlier SR work was developed in the frequency domain using discrete Fourier transform (DFT), such as the work of Tsai and Huang [1], Kim et al. [2,3] and so on. More recently, discrete cosine transform (DCT) [4] and wavelet transform based SR methods [5–7] have also been proposed. In the spatial domain, typical reconstruction models include non-uniform interpolation [8], iterative back projection (IBP) [9], projection onto convex sets (POCS) [10–13], maximum likelihood (ML) [14], maximum *a posteriori* (MAP) [15–17], hybrid ML/MAP/POCS [18], and adaptive filtering [19]. Based on these basic reconstruction models, researchers have produced many extended algorithms, such as the joint formulation of reconstruction and registration [20–23], algorithms for multi-spectral and color [24,25], hyper-spectral [26], and compressed [27,28] sequence, etc. Amongst the numerous solution techniques featuring in the literature, the MAP estimation method is one of the most promising.

In many surveillance video applications, it is of interest to recognize an object that is selected as a region of interest (ROI), such as numbers, words, or labels that often occupy a small portion of a low-resolution, noisy video [29]. In these circumstances, edges of the object are often very useful and important for surveillance applications, but the commonly used Gaussian

* Corresponding author. Tel.: +86 27 68778452; fax: +86 27 68778229.
E-mail address: zlp62@lmars.whu.edu.cn (L. Zhang).

0165-1684/$ - see front matter © 2009 Elsevier B.V. All rights reserved.
doi:10.1016/j.sigpro.2009.09.002

Markov random field regularization (GMRF) in the MAP-based SR cannot effectively preserve sharp edges in the estimated images. To achieve this, several edge-preserving regularizations have been proposed, such as Huber–Markov regularization [15] and bilateral-TV regularization [30]. This paper proposes a weighted directional Markov image prior model, which utilizes different weights for different directional smoothness measures of the edge pixels to reduce the smoothing effect of the common Markov random field prior along edges. Conjugate gradient optimization is then developed to estimate the HR image. Standard operations on images such as convolution, warping, sampling are used to improve the computational efficiency of the algorithm. Experimental results show that the proposed algorithm can effectively preserve edges and detailed information in the reconstructed image.

The rest of the paper is organized as follows. Section 2 presents the image observation model of the SR problem. The motion estimation method employed is described in Section 3. In Section 4, the MAP estimation based reconstruction algorithm is explained. Experimental results are provided in Section 5, and Section 6 concludes this paper.

2. Image observation model

The image observation model is employed to relate the desired referenced HR image to all the observed LR images. Typically, the imaging process involves warping, followed by blurring and down-sampling to generate LR images from the HR image. Let the underlying HR image be denoted in the vector form by $z=[z_1,z_2,\ldots,z_{L_1N_1\times L_2N_2}]^T$, where $L_1N_1\times L_2N_2$ is the HR image size. Letting L_1 and L_2 denote the down-sampling factors in the horizontal and vertical directions, respectively, each observed LR image has the size $N_1\times N_2$. Thus, the LR image can be represented as $y_k=[y_{k,1},y_{k,2},\ldots,y_{k,N_1\times N_2}]^T$, where $k=1,2,\ldots,P$, with P being the number of LR images. Assuming that each observed image is contaminated by additive noise, the observation model can be represented as [18]

$$y_k = DB_kM_kz + n_k \tag{1}$$

where M_k is the warp matrix with the size of $L_1N_1L_2N_2\times L_1N_1L_2N_2$, B_k represents the camera blur matrix also of size $L_1N_1L_2N_2\times L_1N_1L_2N_2$, D is a $N_1N_2\times L_1N_1L_2N_2$ down-sampling matrix, and n_k represents the $N_1N_2\times 1$ noise vector. It should be noted that all the images are assumed to have the same blurring function, so the matrix B_k can be substituted by B

$$y_k = DBM_kz + n_k = A_kz + n_k \tag{2}$$

Fig. 1 illustrates this equation.

3. Motion estimation method

Motion estimation/registration plays a critical role in SR reconstruction, where it is necessary to select a frame from the sequence as the reference one. In general, the sub-pixel motions between the reference frame and the unreferenced frame can be modeled and estimated by a parameter model. This section introduces the motion estimation methods employed.

It is assumed that the motion of the ROI during the sequence is a globally translational motion and the motions of all points can often be modeled by a parametric model. Generally, the relationship between the observed kth and lth frames can be expressed by

$$y_k(x_u,x_v) = y_k^{'(l,\theta)}(x_u,x_v) + \varepsilon_{l,k}(x_u,x_v) \tag{3}$$

where (x_u,x_v) denotes the pixel site, $y_k(x_u,x_v)$ is a pixel in frame k, θ is the vector containing the corresponding motion parameters, $y_k^{'(l,\theta)}(x_u,x_v)$ is the predicted pixel of $y_k(x_u,x_v)$ from frame l using parameter vector θ, and $\varepsilon_{l,k}(x_u,x_v)$ denotes the model error. In the literature, the six-parameter affine model and eight-parameter perspective model are widely used. Here the concentration is on the affine model, in which $y_k^{'(l,\theta)}(x_u,x_v)$ can be expressed as

$$y_k^{'(l,\theta)}(x_u,x_v) = y_l(a_0+a_1x_u+a_2x_v, b_0+b_1x_u+b_2x_v) \tag{4}$$

In this model, $\theta=(a_0,a_1,a_2,b_0,b_1,b_2)^T$ contains six geometric model parameters. To solve θ, we can employ the least square criteria, which has the following minimization cost function:

$$E(\theta) = \|y_k - y_k^{'(l,\theta)}\|^2 \tag{5}$$

Using the Gauss–Newton method, the six affine parameters can be iteratively solved by

$$\Delta\theta = [(J^n)^TJ^n]^{-1}[-(J^n)^Tr^n] \tag{6}$$

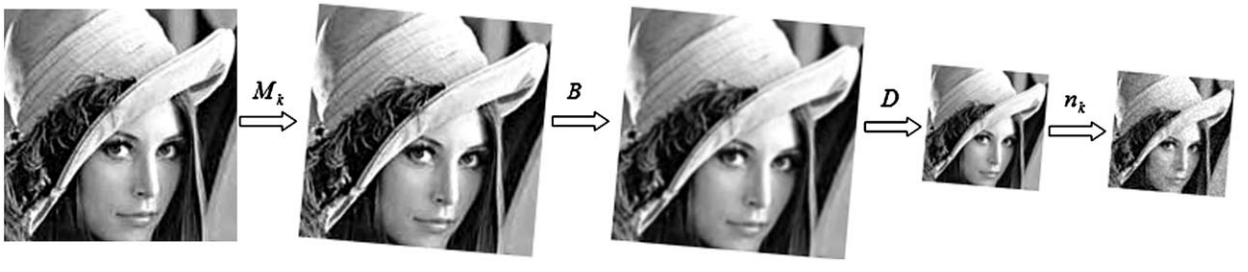

Fig. 1. Block diagram illustration of the observation model (2), where the desired high-resolution image is at the extreme left with the observed image at the extreme right.

and

$$\theta^{n+1} = \theta^n + \Delta\theta \tag{7}$$

Here, n is the iteration number, $\Delta\theta$ denotes the corrections of the model parameters, r^n is the residual vector that is equal to $y_k - y_k^{'(l,\theta_n)}$, and $J^n = \partial r^n/\partial\theta^n$ denotes the gradient matrix of r^n.

4. Image reconstruction algorithm

4.1. MAP formulation

In most situations, the problem of SR is an ill-posed inverse one because the information contained in the observed LR images is not sufficient to solve the HR image. In order to obtain more desirable SR results, the ill-posed problem should be stabilized to be well-posed. The MAP method, which can easily include image prior or regularization, is a good framework to describe the SR problem from the statistical point of view. Let the full set of P LR images be denoted by $y = [y_1^T, y_2^T, \ldots, y_P^T]^T$. The purpose is to realize the MAP estimate of HR image z, given the observed LR images y. The estimate can be computed by

$$\hat{z} = \arg\max p(z|y) \tag{8}$$

Applying Bayes' rule, Eq. (8) becomes

$$\hat{z} = \arg\max \frac{p(y|z)p(z)}{p(y)} \tag{9}$$

Since $p(y)$ can be considered a constant and can be eliminated from the optimization in Eq. (9), it can be rewritten as

$$\hat{z} = \arg\max p(y|z)p(z) \tag{10}$$

Assuming the LR images are independent, we obtain

$$\hat{z} = \arg\max[\prod_k p(y_k|z)p(z)] \tag{11}$$

Using the monotonic logarithm function, it can be expressed as

$$\hat{z} = \arg\max[\sum_k \log p(y_k|z) + \log p(z)] \tag{12}$$

Usually, the noise n_k in (1) is assumed to be one of the zero mean white Gaussian types; thus the likelihood distribution $p(y_k|z)$ has the form

$$p(y_k|z) = \frac{1}{C_1}\exp\left(-\frac{\|y_k - A_k z\|^2}{2\sigma_k^2}\right) \tag{13}$$

where C_1 is a constant, and σ_k^2 is the error variance. The image prior $p(z)$ in (12) has the Gibbs form

$$p(z) = \frac{1}{C_2}\exp(-\Gamma(z)) \tag{14}$$

where C_2 is also a constant, and $\Gamma(z)$ is the prior energy functional. Substituting (13) and (14) in (12), after some manipulation, C_1, C_2, and σ_k^2 can be safely dropped, and the maximization of this posterior probability distribution is equivalent to the following regularization problem:

$$\hat{z} = \arg\min[\sum_k \|y_k - A_k z\|^2 + \lambda\Gamma(z)] \tag{15}$$

where the first term $\sum_k \|y_k - A_k z\|^2$ is the data fidelity term, $\Gamma(z)$ acts as the regularization term, and λ is the regularization parameter.

4.2. Weighted directional Markov regularization

For the regularization term, Tikhonov regularization [16,18,21,27,28] and Gauss–Markov [20] are commonly employed. A common criticism of these regularization methods is that the sharp edges and detailed information in the estimates tend to be overly smoothed [31]. Here, a weighted directional Markov regularization is proposed to preserve the edges and detailed information in the reconstruction process.

The energy functional of the common Markov random field is defined as

$$\Gamma(z) = \sum_{c\in C} V_c(z) = \sum_{i=0}^{L_1N_1-1}\sum_{j=0}^{L_2N_2-1}\sum_{m=1}^{4}\rho(d_{i,j}^m z) \tag{16}$$

where $V_c(\cdot)$ is some function of a local group of points c called cliques, and C denotes the set of all cliques throughout the image, $\rho(\cdot)$ is the function of smooth measure $d_{i,j}^m z$, $\rho(\cdot)$ can use a quadratic function or a Huber function, which correspond to Gauss–Markov regularization and Huber–Markov, respectively.

$d_{i,j}^m z$ denotes the directional smooth measures at pixel $z_{i,j}$, and they are given as

$$d_{i,j}^1 x = x_{i,j+1} - 2x_{i,j} + x_{i,j-1}$$

$$d_{i,j}^2 x = \frac{\sqrt{2}}{2}(x_{i-1,j-1} - 2x_{i,j} + x_{i+1,j+1})$$

$$d_{i,j}^3 x = x_{i+1,j} - 2x_{i,j} + x_{i-1,j}$$

$$d_{i,j}^4 x = \frac{\sqrt{2}}{2}(x_{i-1,j+1} - 2x_{i,j} + x_{i+1,j-1}) \tag{17}$$

It is noted that the intensity difference between the pixels perpendicular to the image edges is larger, while that between the pixels along the edges is smaller. The traditional MRF regularization poses the same constraint coefficients for the four directional smooth measures, with the same extent constraint to the central edge pixel from the neighborhood pixels, which causes the sharp edges and detailed information in the estimated image to be overly smoothed. To preserve the sharp edges in the estimate, the constraint between the pixels perpendicular to the edges should be reduced and that between the pixels along the edges should be increased. For this, the weighted Markov random field (WMRF) regularization is proposed to preserve the sharp edges.

The energy functional of the WMRF is defined as

$$\Gamma(z) = \sum_{c\in C} V_c(z) = \sum_{i=0}^{L_1N_1-1}\sum_{j=0}^{L_2N_2-1}\sum_{m=1}^{4} w_m\rho(d_{i,j}^m z) \tag{18}$$

where w_m ($m = 1,2,3,4$) are the positive weight coefficients for the directional smooth measure.

The Prewit operators are first used to detect edge pixels in the image. For the non-edge pixels, the four weights are set to $w_1 = w_2 = w_3 = w_4 = 1$; while for the edge pixels,

the weights should satisfy the following properties: (a) the weights w_k should be inversely proportional to the smooth measure function $\rho(d^m_{i,j}z)$; (b) $\sum_{m=1}^{4} w_m = 4$. This constraint avoids the trivial solution (all zeros) for w_m. The simplest linear solution for criteria (a) and (b) is

$$w_m = \frac{R_{ave}}{\rho(d^m_{i,j,z}) + \beta} \tag{19}$$

where β is a small positive parameter, which prevents the denominator from becoming zero. R_{ave} is defined as

$$R_{ave} = \frac{4}{\sum_{m=1}^{4} \frac{1}{\rho(d^m_{i,j,z})+\beta}} \tag{20}$$

w_m depends on the smooth measure at pixel $z_{i,j}$.

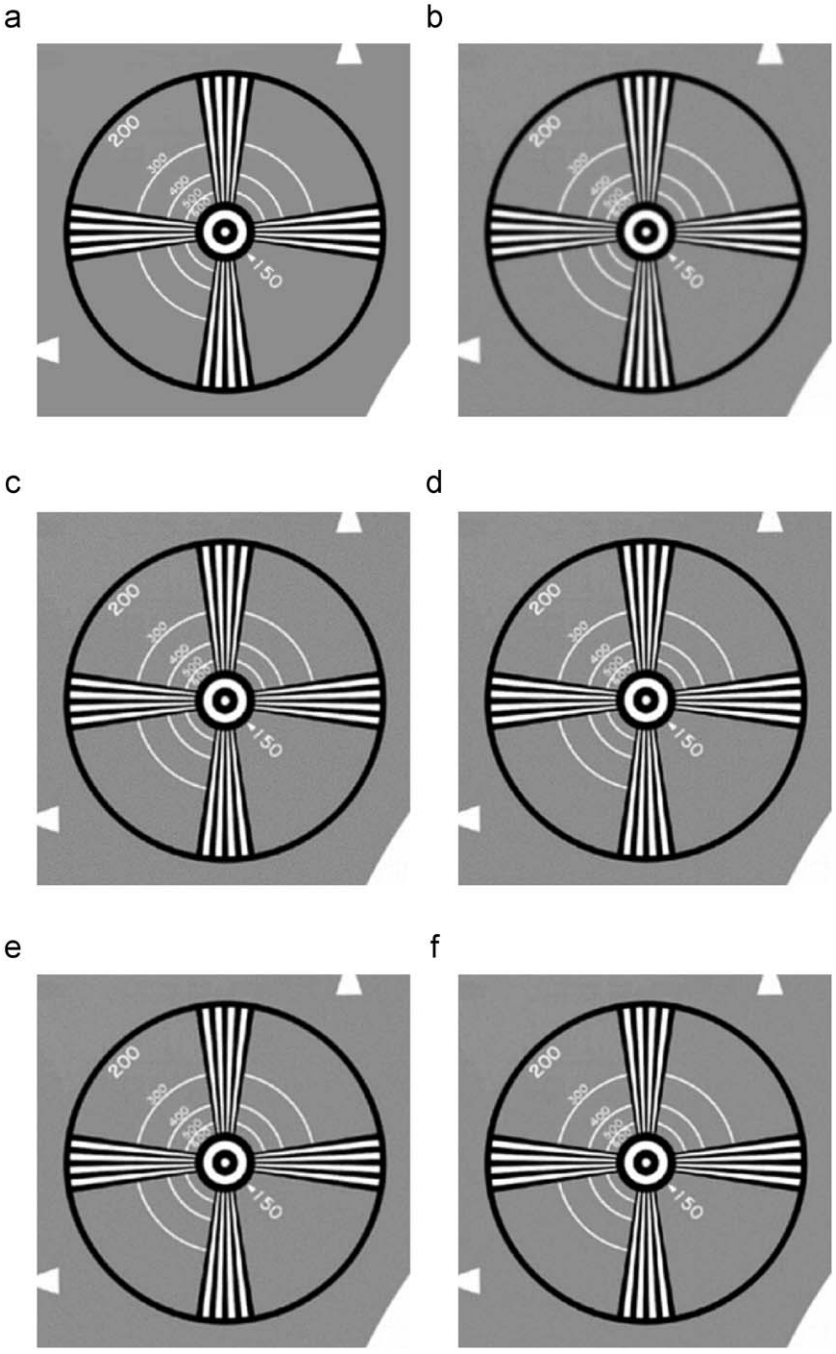

Fig. 2. Simulation results of deblurring using different regularizations. (a) Original image. (b) Blurred and noisy image. (c) Deblurring result with GMRF regularization. (d) Deblurring result with GWMRF regularization. (e) Deblurring result with HMRF regularization. (f) Deblurring result with HWMRF regularization.

4.3. Numerical solution

It is time-consuming to solve the super-resolution problem in the form of matrix-vector because of the very high dimensionality of vector z. A considerable speedup in the super-resolution computation can be achieved by taking advantage of the following two methods: implementing advanced gradient based optimization techniques and computing the gradient in an efficient manner.

In this paper, we derive the conjugate gradient (CG) optimization method to solve the cost function (15). The CG optimization utilizes conjugate direction instead of local gradient to search for the minima. Therefore, it can achieve faster convergence when compared to the steepest descent method [32]. It also requires less storage requirements and computation complexity compared with the Quasi-Newton method.

The gradient of the cost function is denoted as $r(\hat{z}^n) = \sum_k A_k^T(A_k\hat{z}^n - y_k) + \lambda\nabla\Gamma(\hat{z}^n)$. The right term of the gradient $\nabla\Gamma(\hat{z}^n)$ is the derivative of the regularization term with respect to z and can be approximated from the estimated HR image. While the left term $A_k^T(A_k\hat{z}^n - y_k) = M_k^T B^T D^T(DBM_k\hat{z}^n - y_k)$ can be computed using basic image operations such as warp, blur, and sampling instead of

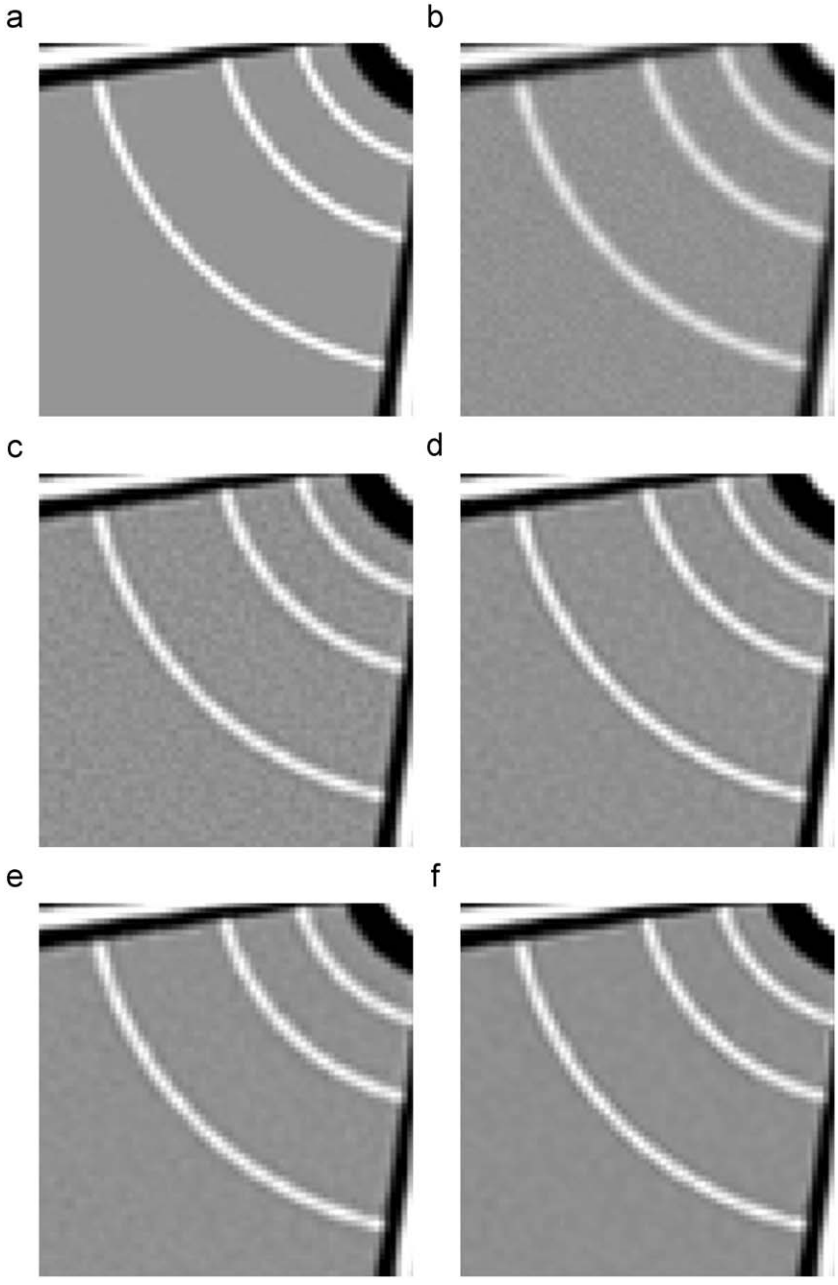

Fig. 3. (a–f) Detail regions cropped from Fig. 2(a–f), respectively.

Table 1
The MSE errors of super-resolution reconstruction using different regularizations.

	GMRF	GWMRF	HMRF	HWMRF
First experiment	18.79	14.61	12.91	9.73
Second experiment	77.54	72.02	71.85	62.51

sparse matrices multiplications. The matrices M_k, B, D model the image formation process, and their implementation is simply the image warping, blurring, and down-sampling, respectively. The implementation of their transpose matrices is also very simple. D^T is implemented by up-sampling the image without interpolation, i.e., by zero padding. For a convolution blur, B^T is implemented by convolution with the flipped kernel of the imaging blur

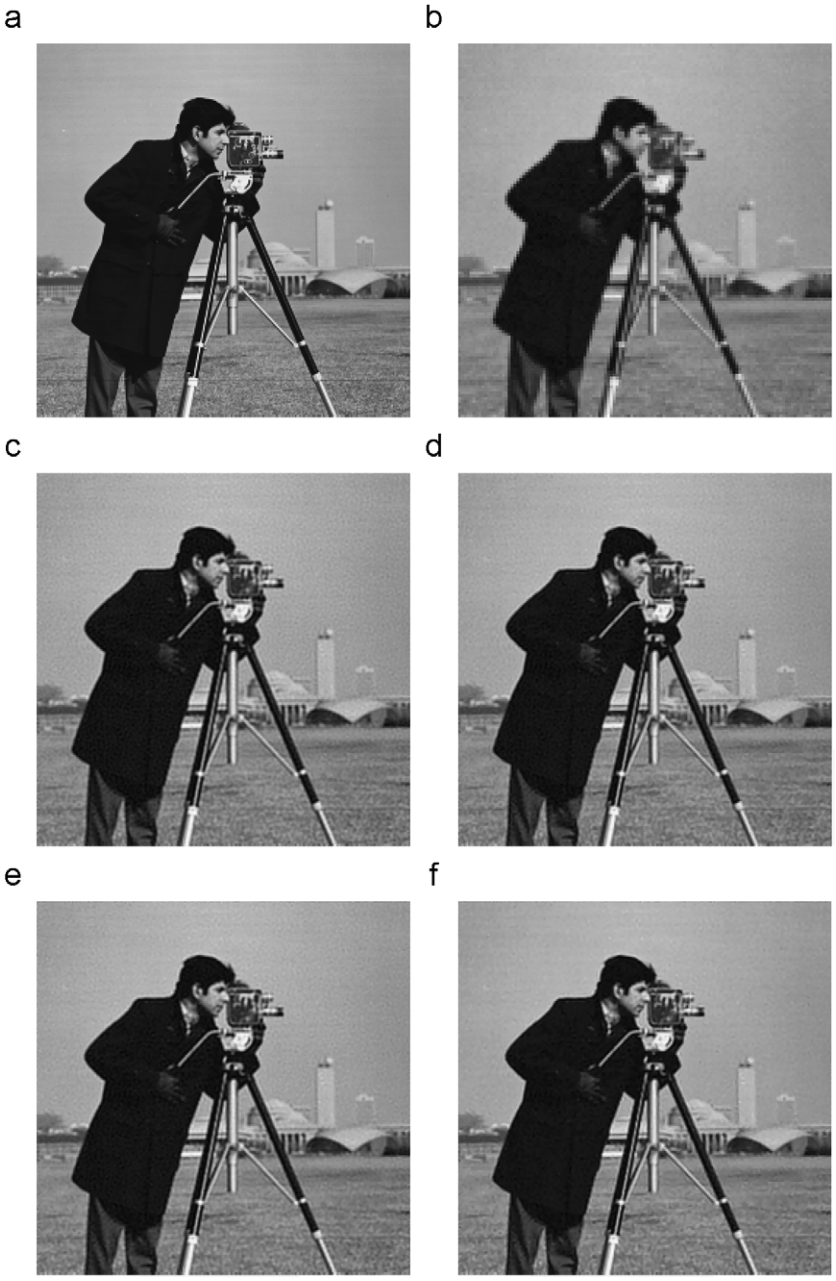

Fig. 4. Results of super-resolution reconstruction using different regularizations. (a) Original image. (b) LR image. (c) Reconstruction result with GMRF regularization. (d) Reconstruction result with GWMRF regularization. (e) Reconstruction result with HMRF regularization. (f) Reconstruction result with HWMRF regularization.

kernel $b(i,j)$. If M_k is implemented by backward warping, then M_k^T should be the forward warping of the inverse motion [33]. Thus, the gradient of the cost function with the WMRF regularization is computed in an efficient manner and the CG optimization technique can be used without explicit construction of these large matrices.

5. Experiments

To test the performance of the proposed algorithm, a number of experiments were conducted, four of which are presented here. The first two were controlled simulated experiments, and the last two were real surveillance image sequences with unknown motion vectors. The following mean square error (MSE) [34] was employed as the quantitative measure:

$$MSE = \frac{\|z - \hat{z}\|^2}{L_1N_1 \times L_2N_2} \tag{22}$$

where $L_1N_1L_2N_2$ is the total number of pixels in the HR image, $\hat{z}$ and z represent the reconstructed HR image and the original image, respectively. Here the quadratic

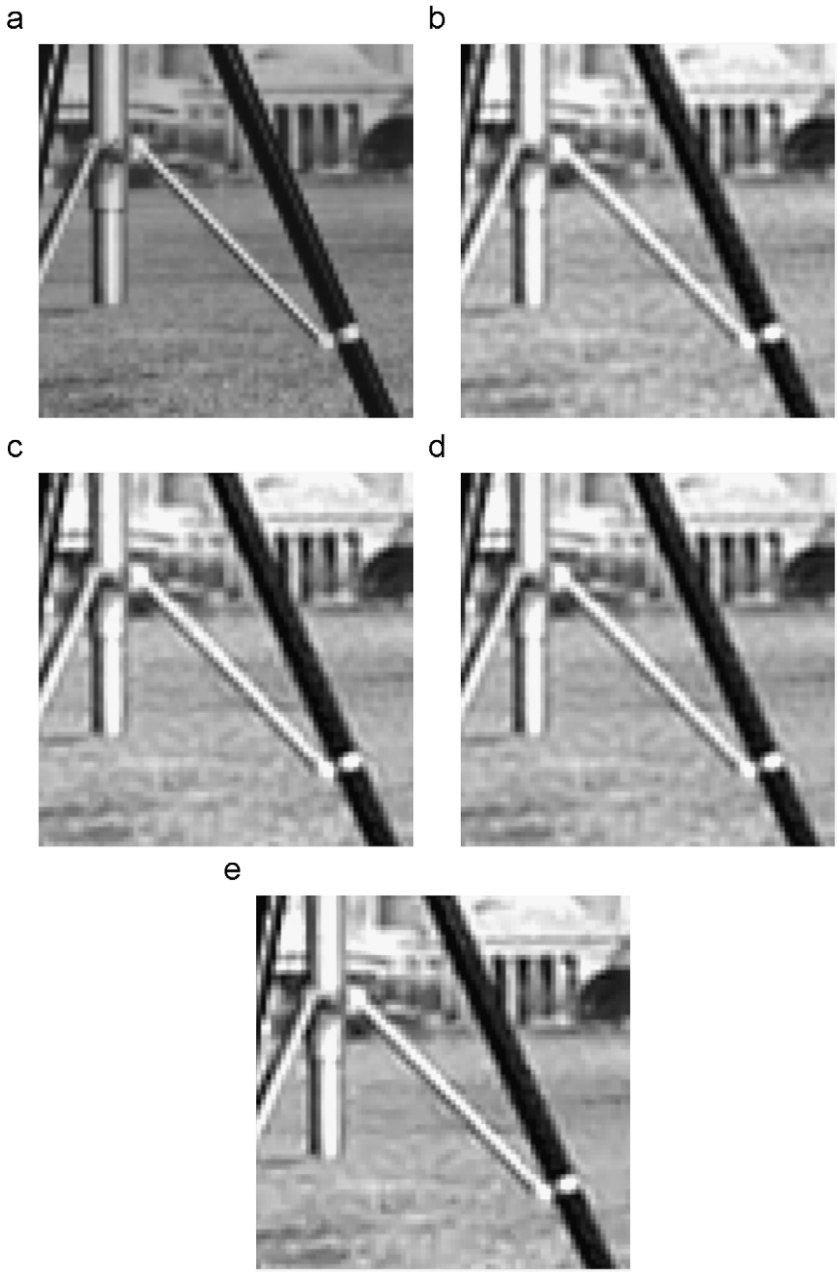

Fig. 5. (a–e) Detailed regions cropped from Fig. 4(a, c–f), respectively.

function and the Huber function are both chosen as the function of smooth measure to compare the performance of MRF and WMRF regularizations.

5.1. Controlled simulated experiments

In the first experiment, the superiority of the WMRF regularization over MRF regularization was justified. We corrupted an image by blurring it with a 3×3 Gaussian blur kernel with standard deviation equal to 0.5. Gaussian additive noise was added to the resulting blurred image to achieve SNR equal to 25 dB. If z and y represent the original and corrupted images, and B represents the matrix of blur kernel, the blurred noisy image can be reconstructed by minimizing the following:

$$\hat{z} = \arg\min[\|y - Bz\|^2 + \lambda\Gamma(z)] \tag{23}$$

The criterion for regularization parameter selection in this experiment was to choose parameters that produced the most visually appealing results. Therefore, to ensure fairness, each method was repeated several times with different regularization parameters and the best result was chosen as the output of the method [30].

Figs. 2(a) and 3(a) show the original image and its zoom. Figs. 2(b) and 3(b) are the corrupted $y = Bz + n$, where n is the Gaussian additive noise. The image was reconstructed using MRF and WMRF regularizations, and this scenario can be thought of as a super-resolution reconstruction problem with a resolution enhancement factor of one.

The reconstruction results are shown in Figs. 2 and 3. The MSE errors of these results are listed in Table 1. The selected threshold for Prewit operators is set to 35. When the quadratic function is chosen as the function of the smooth measure, the reconstruction result of GMRF regularization is shown in Figs. 2(c), 3(c) and achieves the smallest MSE error of 18.79; while Figs. 2(d) and 3(d) are the reconstruction result of the proposed GWMRF regularization, which has the best MSE value of 14.61. When using the Huber function as the function of the smooth measure, the reconstruction result of the edge-preserving HMRF regularization proposed in [15] is shown in Figs. 2(e), 3(e) and has the smallest MSE error of 12.91; the proposed HWMRF regularization achieves the MSE error of 9.73, and the reconstructed image is shown in Figs. 2(f) and 3(f). From the comparison of Fig. 3(c–f), the reconstruction result of GWMRF regularization is better than GMRF and close to HMRF, while HWMRF achieves the best result. We notice that whichever function is chosen as the function of the smooth measure, the proposed WMRF regularization achieves better results than MRF regularization in terms of both the quantitative measurements and visual evaluation.

Our second experiment uses "Cameraman" image to validate the performance of our proposed algorithm. In this experiment, a sequence of LR frames was created by using one HR image shown in Fig. 4(a). First, this HR image was shifted by one pixel in the vertical direction. Then, to simulate the effect of camera PSF, this shifted image was convolved with a symmetric Gaussian blur kernel of size 5×5 with standard deviation equal to 0.5. The resulting image was downsampled by the factor of 2 in each direction. The same approach with different motion vectors in the vertical and horizontal directions was used to produce four LR images from the original scene. Gaussian noise was added to the resulting LR images to achieve a signal-to-noise ratio (SNR) equal to 27 dB. One of these LR images is presented in Fig. 4(b).

We used these four LR noisy images with a resolution enhancement factor of 2 in this experiment. The results of the super-resolution reconstruction are shown in Figs. 4 and 5. The MSE errors of these results are listed in Table 1. The selected threshold for Prewit operators is 30. When using the quadratic function as the function of the smooth measure, MSE values of GMRF and GWMRF regularization are equal to 77.54 and 72.02, respectively. The corresponding result images are shown in Fig. 4(c) and (d), respectively. Detailed regions cropped from Fig. 4(c) and (d) are shown in Fig. 5(b) and (c), respectively. When using the Huber function, MSE values of HMRF and HWMRF regularization are equal to 71.85 and 62.51, respectively. The corresponding results are shown in Fig. 4(e) and (f), respectively. Detailed regions cropped from Fig. 4(e) and (f) are shown in Fig. 5(d) and (e), respectively. It is evident that the proposed WMRF regularization outperforms the conventional MRF regularization in terms of both the quantitative measurement and visual evaluation.

5.2. Surveillance sequences

Here we use real surveillance sequences to validate the effectiveness of the proposed super-resolution method. It is assumed that the motion of the images during the sequence is a globally translational motion; the motions between the reference image and the unreferenced images can be estimated by the affine parameter model introduced in Section 3.

The first surveillance sequence experiment shows a SR reconstruction of a car sequence, which was obtained from a surveillance video camera. One frame of this

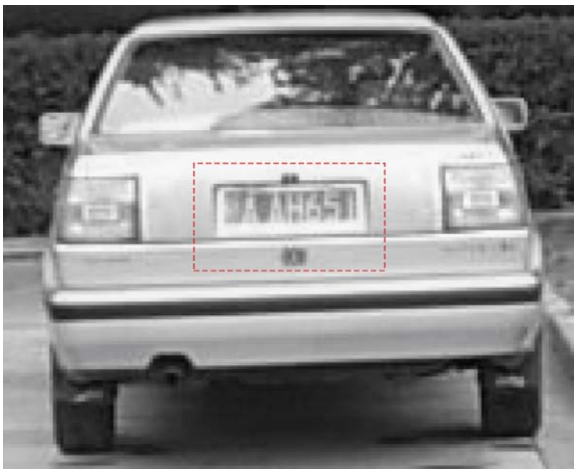

Fig. 6. One frame in the car video. The car license plate boxed in dashes is the selected ROI.

sequence is shown in Fig. 6. Here the car license plate is selected as our ROI. We used five LR images with frame 1 (the referenced frame) shown in Fig. 7(a) to obtain a resolution enhancement factor of 2. The camera blur kernel is assumed to be a 5×5 Gaussian kernel with a standard deviation equal to 0.5. The selected threshold for Prewit operators is 60. Fig. 7(b–d) shows the bilinear interpolated image, the SR result using HMRF regularization, and the result with HWMRF regularization, respectively. Detailed regions cropped from Fig. 7(b–d) are

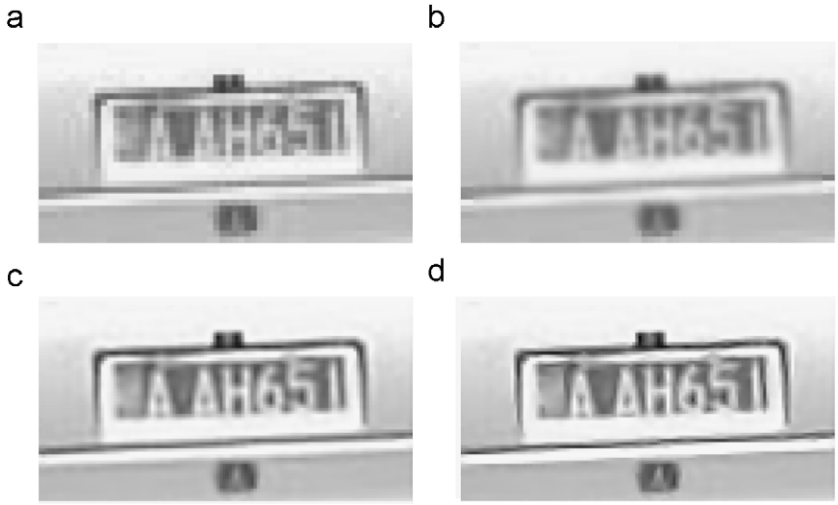

Fig. 7. Results of super-resolution reconstruction using different regularizations. (a) Frame 1 of the surveillance sequence. (b) Bilinear interpolation. (c) SR result with HMRF regularization. (d) SR result with HWMRF regularization.

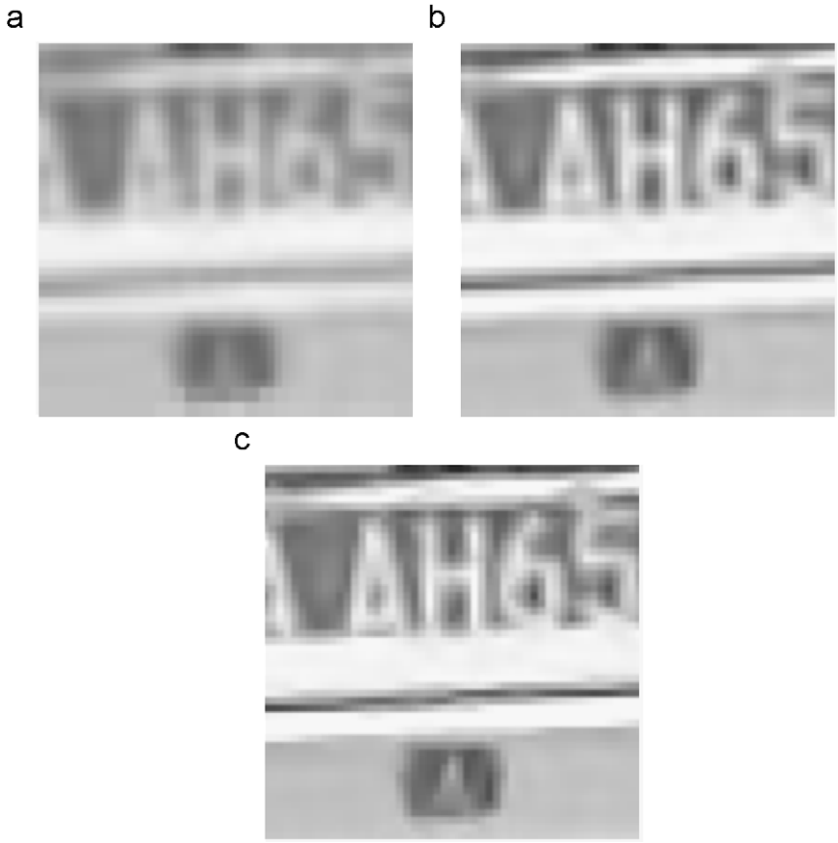

Fig. 8. (a–c) Detailed regions cropped from Fig. 7(b–d), respectively.

shown in Fig. 8(a–c), respectively. Evidently, the proposed algorithm using HWMRF regularization has better visual quality than the conventional MAP algorithm with HMRF regularization.

Our second real experiment uses the disk surveillance sequence. Here we used five frames with frame 1 (the referenced frame) which is shown in Fig. 9(a). The camera blur kernel is assumed to be a 5×5 Gaussian kernel with

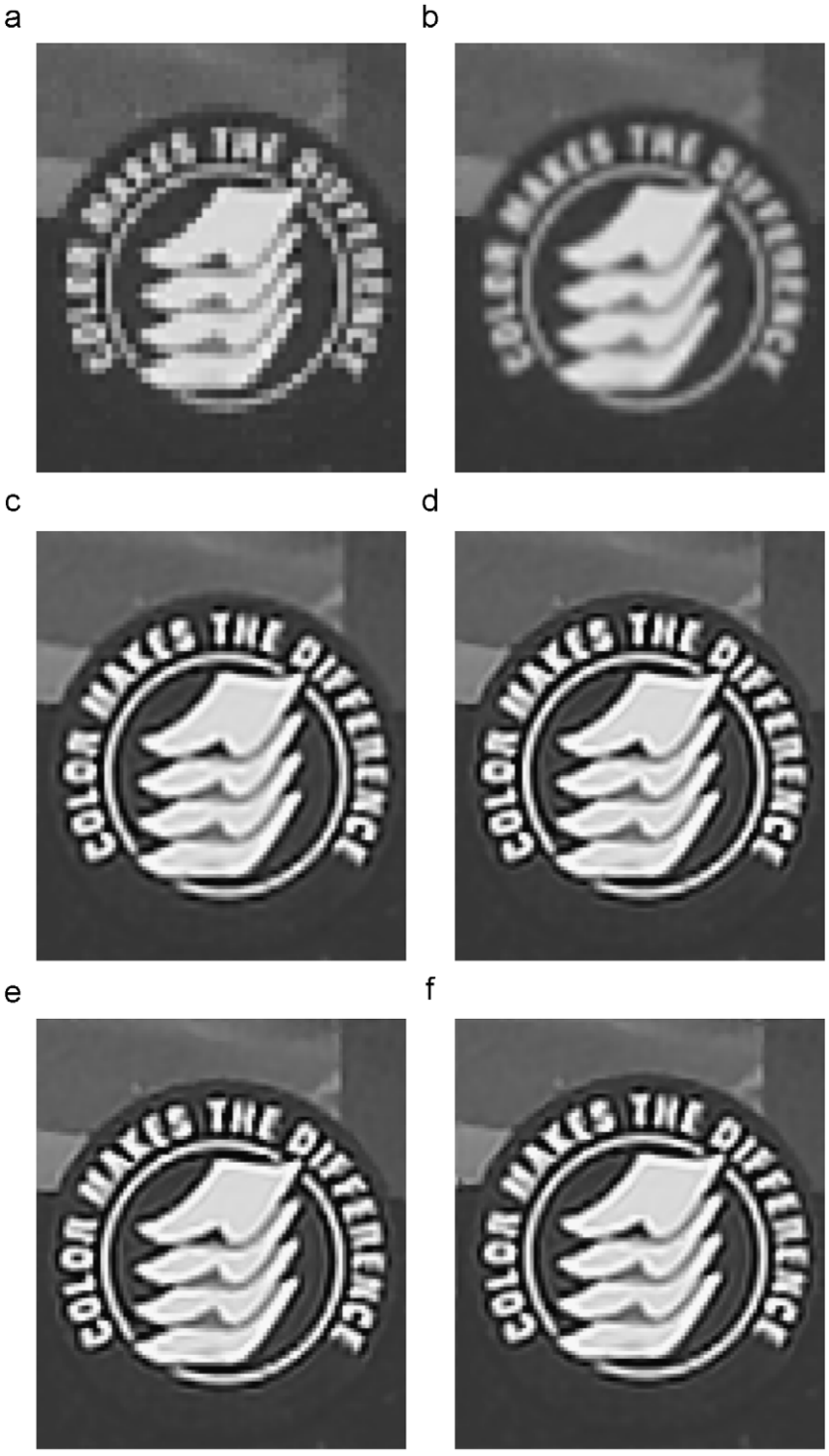

Fig. 9. Results of super-resolution reconstruction using different regularizations. (a) Frame 1 of the surveillance sequence. (b) Bilinear interpolation. (c) SR result with HMRF regularization. (d) SR result with HWMRF regularization. (e) SR result with HWMRF regularization of frame 3. (f) SR result with HWMRF regularization of frame 5.

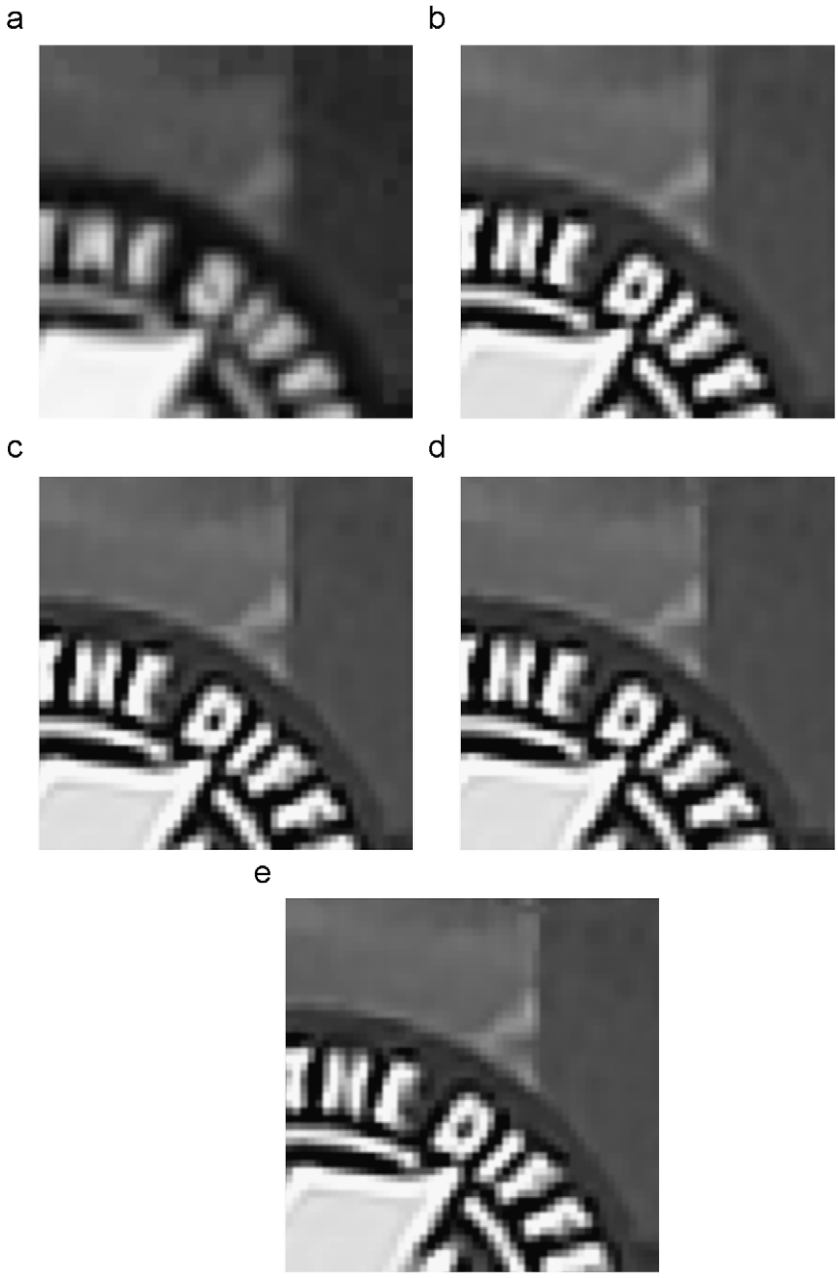

Fig. 10. (a–e) Detailed regions cropped from Fig. 7(b–f), respectively.

a standard deviation equal to 0.5. The selected threshold for Prewit operators is set to 30. Fig. 9(b–d) shows the bilinear interpolated image, the SR result using HMRF regularization, and the result with HWMRF regularization, respectively. Detailed regions cropped from Fig. 9(b–d) are shown in Fig. 10(a–c), respectively. It is apparent that the proposed algorithm using HWMRF regularization obtained more desirable result than the bilinear interpolation and the conventional MAP algorithm with HMRF regularization. Other frames of the surveillance sequence can also be selected as the referenced frame, so that we can obtain a HR surveillance sequence. SR reconstruction results of frames 3 and 5 are showed in Fig. 9(e–f), respectively. Detailed regions cropped from Fig. 9(e–f) are shown in Fig. 10(d–e), respectively.

6. Conclusions

This paper proposes an edge-preserving MAP estimation based super-resolution algorithm by using the weighted Markov random field regularization for a ROI from several low-resolution surveillance images. The motion of the ROI during the sequence is assumed to

be globally translational and estimated by a parameter model. CG optimization based on standard operations on images such as convolution, warping, and sampling is used to speedup the super-resolution computation. The proposed algorithm was tested on different series of synthetic images and real surveillance sequences. Experimental results validated that the proposed algorithm outperforms interpolation methods and conventional MAP algorithm with HMRF regularization in terms of both the quantitative measurements and visual evaluation.

Acknowledgments

We want to thank the helpful comments and suggestions from the anonymous reviewers. This work was supported by Major State Basic Research Development Program (973 Program) of China under Grant No. 2009CB723905, the National High Technology Research and Development Program (863 Program) of China under Grant Nos.2009AA12Z114, 2007AA12Z148, the National Natural Science Foundation of China under Grant Nos. 40930532, 40801182, 40771139, 40523005, 40721001.

References

[1] R.Y. Tsai, T.S. Huang, Multi-frame image restoration and registration, Advances in Computer Vision and Image Processing 1 (1984) 317–339.
[2] S.P. Kim, N.K. Bose, H.M. Valenzuela, Recursive reconstruction of high resolution image from noisy undersampled multiframes, IEEE Transactions on Acoustics, Speech, and Signal Processing 38 (6) (1990) 1013–1027.
[3] S.P. Kim, W.Y. Su, Recursive high-resolution reconstruction of blurred multiframe images, IEEE Transactions of Image Processing 2 (4) (1993) 534–539.
[4] S. Rhee, M.G. Kang, Discrete cosine transform based regularized high-resolution image reconstruction algorithm, Optical Engineering 38 (8) (1999) 1348–1356.
[5] R. Chan, T. Chan, L. Shen, Z. Shen, Wavelet algorithms for high-resolution image reconstruction, SIAM Journal on Scientific Computing 24 (4) (2003) 1408–1432.
[6] S. Lertrattanapanich, N.K. Bose, High resolution image formation from low resolution frames using Delaunay triangulation, IEEE Transactions on Image Processing 11 (12) (2002) 1427–1441.
[7] M.K. Ng, C.K. Sze, S.P. Yung, Wavelet algorithms for deblurring models, International Journal of Imaging Systems and Technology 14 (3) (2004) 113–121.
[8] H. Ur, D. Gross, Improved resolution from sub-pixel shifted pictures, CVGIP: Graphical Models and Image Processing 54 (1992) 181–186.
[9] M. Irani, S. Peleg, Improving resolution by image registration, CVGIP: Graphical Models and Image Processing 53 (3) (1991) 231–239.
[10] H. Stark, P. Oskoui, High-resolution image recovery from image plane arrays, using convex projections, Journal of the Optical Society of America A: Optics and Image Science, and Vision 6 (1989) 1715–1726.
[11] A.M. Tekalp, M.K. Ozkan, M.I. Sezan, High-resolution image reconstruction from lower-resolution image sequences and space-varying image restoration, in: IEEE International Conference of Acoustics, Speech and Signal Processing, 1992, pp. 23–26.
[12] A.J. Patti, M.I. Sezan, A.M. Tekalp, High-resolution image reconstruction from a low-resolution image sequence in the presence of time-varying motion blur, in: IEEE International Conference on Image Processing, 1994, pp. 13–16.
[13] A.J. Patti, M.I. Sezan, A.M. Tekalp, Super-resolution video reconstruction with arbitrary sampling lattices and nonzero aperture time, IEEE Transactions on Image Processing 6 (8) (1997) 1064–1076.
[14] B.C. Tom, A.K. Katsaggelos, Reconstruction of a high-resolution image from multiple-degraded mis-registered low-resolution images, in: SPIE—The International Society for Optical Engineering, 1994, pp. 971–981.
[15] R.R. Schultz, R.L. Stevenson, Extraction of high-resolution frames from video sequences, IEEE Transactions on Image Processing 5 (6) (1996) 996–1011.
[16] R.C. Hardie, T.R. Tuinstra, J. Bognar, K.J. Barnard, E. Armstrong, High resolution image reconstruction from digital video with global and non-global scene motion, in: IEEE International Conference on Image Processing, 1997, pp. 153–156.
[17] L.C. Pickup, D.P. Capel, S.J. Roberts, A. Zisserman, Bayesian image super-resolution, continued, Advances in Neural Information Processing Systems (2006) 1089–1096.
[18] M. Elad, A. Feuer, Restoration of a single super-resolution image from several blurred, noisy, and undersampled measured images, IEEE Transactions on Image Processing 6 (12) (1997) 1646–1658.
[19] M. Elad, A. Feuer, Super-resolution restoration of an image sequence: adaptive filtering approach, IEEE Transactions on Image Processing 8 (3) (1999) 387–395.
[20] R.C. Hardie, K.J. Barnard, E.E. Armstrong, Joint MAP registration and high-resolution image estimation using a sequence of undersampled images, IEEE Transactions on Image Processing 6 (12) (1997) 1621–1633.
[21] N.A. Woods, N.P. Galatsanos, A.K. Katsaggelos, Stochastic methods for joint registration, restoration, and interpolation of multiple undersampled images, IEEE Transactions on Image Processing 15 (1) (2006) 201–213.
[22] J. Chung, E. Haber, J. Nagy, Numerical methods for coupled super resolution, Inverse Problems 22 (4) (2006) 1261–1272.
[23] H. Shen, L. Zhang, B. Huang, P. Li, A MAP approach for joint motion estimation, segmentation and super resolution, IEEE Transactions on Image Processing 16 (2) (2007) 479–490.
[24] R. Sasahara, H. Hasegawa, I. Yamada, K. Sakaniwa, A color super-resolution with multiple nonsmooth constraints by hybrid steepest descent method, in: IEEE International Conference on Image Processing, 2005, pp. 857–860.
[25] S. Farsiu, M. Elad, P. Milanfar, Multiframe demosaicing and super-resolution of color images, IEEE Transactions on Image Processing 15 (1) (2006) 141–159.
[26] T. Akgun, Y. Altunbasak, R.M. Mersereau, Super-resolution reconstruction of hyperspectral images, IEEE Transactions on Image Processing 14 (11) (2005) 1860–1875.
[27] C.A. Segall, A.K. Katsaggelos, R. Molina, J. Mateos, Bayesian resolution enhancement of compressed video, IEEE Transactions on Image Processing 13 (7) (2004) 898–910.
[28] C.A. Segall, R. Molina, A.K. Katsaggelos, High-resolution images from low-resolution compressed video, IEEE Signal Processing Magazine 20 (3) (2003) 37–48.
[29] G. Canel, A.M. Tekalp, W. Heinzelman, Super resolution recovery for multi-camera surveillance imaging, in: Proceedings of the 2003 IEEE International Conference on Multimedia and Expo (ICME), 2003, pp. 109–112.
[30] S. Farsiu, M.D. Robinson, M. Elad, P. Milanfar, Fast and robust multiframe super resolution, IEEE Transactions on Image Processing 13 (10) (2004) 1327–1344.
[31] M.K. Ng, H. Shen, E. Lam, L. Zhang, A total variation based super-resolution reconstruction algorithm for digital video, EURASIP Journal on Advances in Signal Processing (2007) Article ID 74585, 16pp, doi:10.1155/2007/74585.
[32] Y. He, K.H. Yap, L. Chen, L.P. Chau, A soft MAP framework for blind super-resolution image reconstruction, Image and Vision Computing 27 (4) (2009) 364–373.
[33] A. Zomet, S. Peleg, Super-resolution from multiple images having arbitrary mutual motion, in: S. Chaudhuri (Ed.), Super-Resolution Imaging, Kluwer Academic, New York, 2001, pp. 195–209.
[34] W. Zhou, C. Alan, A. Bovik, Univeral image quality index, IEEE Signal Processing Letters 9 (3) (2002) 81–84.